Large Eddy Simulation of Non-Isothermal Turbulent Rotor-Stator Flows

Sébastien Poncet, Eric Serre

The 12th International Symposium on Transport Phenomena and Dynamics of Rotating Machinery
Honolulu, Hawaii, February 17-22, 2008

ISROMAC12-2008-20009

LARGE EDDY SIMULATION OF NON-ISOTHERMAL TURBULENT ROTOR-STATOR FLOWS

S. Poncet[1], E. Serre[2]

Laboratoire MSNM-GP, UMR 6181 CNRS-Universités Aix-Marseille
Technopôle Château-Gombert, 38 rue F. Joliot-Curie, 13451 Marseille, FRANCE
[1]poncet@l3m.univ-mrs.fr, Tel. 33 (0)4 91 11 85 23, Fax 33 (0)4 91 11 85 02
[2]serre1@l3m.univ-mrs.fr, Tel. 33 (0)4 91 11 85 35, Fax 33 (0)4 91 11 85 02

ABSTRACT

Non-isothermal turbulent flows in an enclosed rotor-stator cavity are here investigated using large eddy simulation (LES). Besides their fundamental importance as three-dimensional prototype flows, such flows arise in many industrial applications and especially in turbomachineries. The LES is performed using a Spectral Vanishing Viscosity technique, which is shown leading to stable discretizations without sacrificing the formal accuracy of the spectral approximation. The LES results have been favorably compared to velocity measurements in the isothermal case. The Boussinesq approximation is then used to take into account the centrifugal-buoyancy effects. The thermal effects have been examined for $Re=\Omega b^2/\nu=10^6$ in a rotor-stator cavity of aspect ratio $G=(b-a)/h=5$ and curvature parameter $R_m=(b-a)/(b+a)=1.8$ (a, b the inner and outer radii of the rotor and h the interdisk spacing) and for Rayleigh numbers up to $Ra=10^8$. These LES results provide accurate, instantaneous quantities which are of interest in understanding the physics of turbulent flows and heat transfers in an interdisk cavity. The averaged results show small effects of density variation on the mean and turbulent fields.

NOMENCLATURE

a,b	the inner and outer radii of the rotor (m)
G	the aspect ratio of the cavity
h	the interdisk spacing (m)
h_1	the convective heat transfer coefficient (W/m²/K)
Nu	the local Nusselt number
P	the pressure (bars)
Pr	the Prandtl number
r,θ,z	the cylindrical coordinates
Ra	the Rayleigh number
Re	the rotational Reynolds number
R_m	the curvature parameter
T	the dimensionless temperature
κ	the thermal diffusivity of the fluid (m²/s)
λ	the fluid conductivity (W/m/K)
ν	the kinematic viscosity of the fluid (m²/s)
Ω	the rotation rate of the rotor (rad/s)

INTRODUCTION

Convective heat transfers are here investigated in an enclosed rotor-stator cavity using large eddy simulation (LES). Non-isothermal rotating disk flows arise in many industrial applications, such as in magnetic storage devices (disk drives), semi conductor manufacturing processes with rotating wafers and other rotating machineries like generator rotors or gas turbine engines. For example, in high-speed rotating gas turbines, the cooling air flow is used to both cooling the disk and preventing the ingestion of hot turbine passage gases into the cavity. A good knowledge of heat transfers and fluid flows in such systems is crucial: an excessive amount of coolant is often supplied to the cavity that imposes an unnecessary penalty on the engine cycle and leads to a loss of efficiency.

At that time, most of the published works have dealt with the fluid flow aspects of turbulent rotor-stator flows (Daily and Nece, 1960; Poncet *et al.*, 2005; Séverac *et al.*, 2007) mainly because of the complexity and the cost of making accurate heat transfer measurements. A large review of the fundamental investigations relevant to heat and mass transfers in rotor-stator or rotating cavities carried out until 1989 has been performed by Owen and Rogers (1989a, b). All these studies showed that the influence of the aspect ratio of the cavity on the distribution of the local Nusselt number along the disks is weak compared to the ones of rotation and coolant flow rate. In the regime IV (turbulent flows with separated

boundary layers) of Daily and Nece (1960), the local Nusselt number depends on the global Reynolds number Re to the power 0.8 and to the Prandtl number to the power 0.6 (see Dorfman, 1963).

More recently, Djaoui *et al.* (1998, 2001) examined the turbulent flow in a rotor-stator cavity of large aspect ratio subjected to a superimposed radial inflow and heat transfer effects. Detailed velocity and Reynolds stress tensor measurements as well as temperature and temperature-velocity correlations have been carried out using a hot and cold wire anemometry technique. The temperature distribution was specified on the stator and heat transfer coefficient controlled with the help of pellicular fluxmeters. They studied in particular the external peripheral geometry effects and the critical importance of the inlet conditions on the mean tangential fluid velocity. They focused also on the dependence of the flow structure and heat transfer effects on the Rossby and Reynolds numbers. Comparisons with an asymptotical formulation based on the assumption of inviscid fluid are displayed and in good agreement with the experimental data. Harmand *et al.* (2000) investigated both the flow structure by Particule Image Velocimetry (PIV) and the heat transfers using a thermally rotor heated by infrared radiation in the case of turbulent rotor-stator flows. The local heat flux distribution from the rotor is identified by solving the Laplace equation by finite difference. The local Nusselt number Nu on the rotor is found to be an increasing function of the Reynolds number and remains almost constant along the radius contrary to the free disk case, where Nu increases from the axis to the periphery of the cavity. Pellé and Harmand (2007) studied the influence of the dimensionless interdisk spacing G on the local Nusselt number. It remains almost constant whatever the Reynolds number for $G \leq 12.5$. They identified four heat transfer regimes corresponding to the four flow regimes of Daily and Nece (1960). They also gave correlations for the local and averaged Nusselt numbers depending on the aspect ratio and the Reynolds number.

The fact that only few experimental data are available in the literature has slowed down the development of advanced heat transfer models. Abe *et al.* (1996) developped a two-equation heat transfer model, which incorporates essential features of second-order modeling. They introduced the Kolmogorov velocity scale to take into account the low Reynolds number effects in the near-wall region and also complex heat transfer fields with flow separation and reattachement. But this model has not been yet implemented for rotating disk flows. The major numerical work is the one of Iacovides and Chew (1992). They have used four different models of turbulence to study the convective heat transfer in three axisymmetric rotating disk cavities with throughflow. Three models were based on a zonal modeling approach and one was based on a mixing-length hypothesis. Their numerical predictions were compared to experimental data available in the literature but none of the four models was entirely successful. Nevertheless, considering overall performance, the k-ε model with the one-equation near-wall treatment is preferred. Schiestel *et al.* (1993) have examined the turbulent flow in a rotating cavity with a radial outward throughflow and heat transfer effects. They compared a standard k-ε low-Reynolds number model and a zonal approach using second-order algebraic stress model in the core of the flow. They showed that second-order modeling is necessary to obtain a detailed near-wall treatment. Recently, Poncet and Schiestel (2007) compared a second order moment closure (Reynolds Stress Model) sensitized to rotation effects to data available in the literature. They considered the temperature as a passive scalar and found a close agreement in the case of an open cavity even for large temperature differences. Finally, all workers concluded that further experimental but also numerical research is required before a mathematical model can be recommanded with any confidence.

As already mentioned, the difficulty and the cost of measurements under severe conditions of rotation and temperature do not allow a full description of the mean and turbulent fields. As a consequence, numerical modeling became a valuable tool for predicting flow structure and heat transfer effects in industrial configurations. Previous works (Poncet and Schiestel, 2007) have shown that second-order modeling is a good way to predict the flow structure in a high-speed rotor-stator cavity with axial inward or outward throughflow. Nevertheless, turbulence modeling does not take into account three-dimensional effects due to highly structured large-scale vortices (Czarny *et al*., 2002), which have a large influence on the resultant heat transfer coefficients at the disk surface. Serre *et al.* (2004) performed some direct numerical simulations (DNS) of non-isothermal transitional flows under the Boussinesq approximation but at a moderate Reynolds number $Re=1.1\times10^5$. They showed that the Rayleigh number has a weak influence on the mean field. The purpose of the present work is to propose, for the first time, three-dimensional accurate calculations of highly turbulent rotor-stator flows under non-isothermal conditions in an actual enclosed cavity. The objective is then to acquire precise knowledge of both the flow structure and the temperature distribution on the disks in order to predict durability and determine the disk dimensions.

The paper is organized as follows: we first describe the geometrical configuration and the numerical modeling. Then, comparisons between the LES calculations and some LDV measurements are performed to show the capability of our numerical approach and to present the base flow in the isothermal case. The influence of the Rayleigh number on the mean and turbulent fields is discussed afterwards. Some LES results of instantaneous quantities are shown and the effects of density variation on the averaged results are investigated. Finally some conclusions and closing remarks are provided.

NUMERICAL MODELING

A spectral vanishing viscosity (SVV) method for LES has been developed for simulating turbulent rotor-stator flows. It has the property to preserve the spectral accuracy of the approximation developed in DNS (Serre *et al.*,2004) and keeps the fast time integration of the DNS because it is condensed in pre-processing jobs. The reader is referred to the paper of Séverac and Serre (2007) for a detailed description of this approach.

Geometrical configuration

We consider the flow contained between two flat disks enclosed by two co-axial cylinders of height h (see Fig.1). The inner cylinder (hub) of radius a is attached to the upper disk (rotor) and both rotate at uniform angular velocity Ω. The outer cylinder (shroud) of radius b is attached to the lower disk (stator) and so both are stationary. We define the dimensionless radial r^* and axial z^* coordinates as: $r^*=(r-a)/(b-a)$ and $z^*=z/h$. Thus, $r^*=0$ on the hub and $r^*=1$ on the shroud. In the same way, $z^*=0$ on the stator and $z^*=1$ on the rotor.

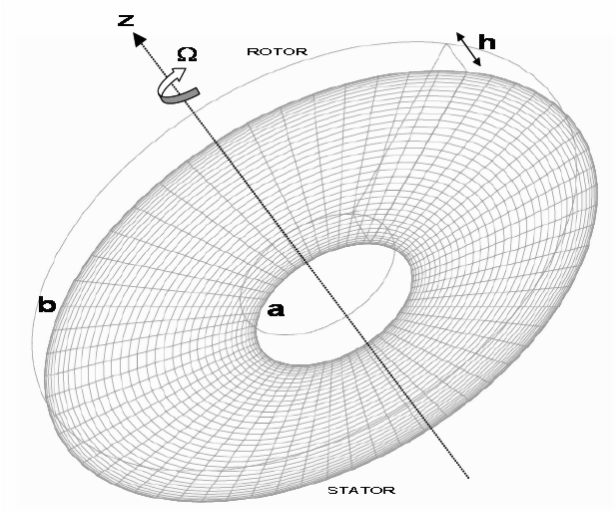

Fig.1: Scheme of the enclosed rotor-stator cavity with relevant notation. Example of the mesh grid within the stator boundary layer (only one-fourth of the points are shown).

In the isothermal case, the mean flow is governed by three main control parameters: the aspect ratio of the cavity G, the curvature parameter R_m and the rotational Reynolds number Re based on the outer radius b of the rotating disk defined as follows:

$$G=(b-a)/h=5$$
$$R_m=(b+a)/(b-a)=1.8$$
$$Re=\Omega b^2/\nu=10^6$$

where ν is the kinematic viscosity of the fluid. The values of the geometrical parameters have been chosen in order to be relevant with industrial devices such as real stage of turbopump, and to satisfy computational effort to reach statistically converged stages. Séverac *et al.* (2007) have performed extensive comparisons in the same geometry for $10^5 \le Re \le 10^6$. In the present work, the value of the Reynolds number is fixed to 10^6 in order to highlight only the thermal effects on the hydrodynamic field.

The temperature is made dimensionless using the temperature difference applied between the stator and the rotor: $T=2(T^*-T_r)/\Delta T$ with $\Delta T=T_{hot}-T_{cold}$ and $T_r=(T_{hot}+T_{cold})/2$. The stator is hot at T=1 and the rotor is cold at T=-1. On the hub and the shroud, insulating conditions with zero heat flux are considered. The Prandtl number Pr and the Rayleigh number based on the maximum radial acceleration Ra have also to be taken into account to study the flow dynamics. They are defined as follows:

$$Pr=\nu/\kappa=0.7$$
$$0 \le Ra=\Omega^2 b\, \Delta T\, h^3 / (\nu\, \kappa\, T_r) \le 10^8$$

where κ is the thermal diffusivity of the fluid. Note that the value of Pr chosen here corresponds to the typical value for air at 20°C. All the parameters are then fixed except for the Rayleigh number, whose influence on the flow dynamics is here investigated.

Mathematical modelling

The motion is governed by the incompressible three-dimensional Navier-Stokes equations written in the velocity-pressure formulation, together with the continuity equation and appropriate boundary conditions. A cylindrical polar coordinate system (r,θ,z) is used. The velocity components are denoted V_r, V_θ and V_z and p is the pressure. The velocity, space and time scalings correspond to Ωb, h and $1/\Omega$ respectively. In the meridional plane, the space variables (r,z) in [a,b] × [0,h] have been normalized into the square [-1,1] × [-1,1], a prerequisite for the use of Chebyshev polynomials.

Numerical method

The pseudospectral numerical method is based on a collocation-Chebyshev method in the r and z non-homogeneous directions and a Galerkin-Fourier method in the azimuthal periodic direction θ. Thus, each dependent variable $f=(V_r,V_\theta,V_z,p)$ is expanded into a truncated trigonometric series:

$$f_{NMK}(r,\theta,z,t)=\sum_{n=0}^{N-1}\sum_{m=0}^{M-1}\sum_{k=-K/2}^{K/2-1}\hat{f}_{nmk}(t)T_n(r)T_m(z)e^{ik\theta} \qquad (1)$$

where T_n and T_m are Chebyshev polynomials of degrees n and m respectively. N, M define the number of collocation points in the radial and axial directions, respectively and K is the cutoff in the tangential direction. To ensure high accuracy of the solution within the very thin wall layers, this approximation is applied at the Gauss-Lobatto collocation points, where the differential equations are assumed to be satisfied exactly: $r_i = \cos(i\pi/N)$ for i in [0,N] and $z_j = \cos(j\pi/M)$ for j in [0,M] in the radial and axial directions. In the azimuthal direction, an uniform distribution is considered: $\theta_k = 2k\pi/K$ for k in [0,K[.

The time scheme is semi-implicit and second order accurate. It is a combination of an explicit treatment of the

convective terms (Adams-Bashforth scheme) and of an implicit treatment for the diffusive terms (second order backward Euler scheme). The solution method is based on an efficient projection scheme to solve the coupling between velocity and pressure. This algorithm ensures a divergence-free velocity field at each time step, maintains the order of accuracy of the time scheme for each dependent variable and does not require the use of staggered grids. Finally, for each Fourier mode, a full diagonalization technique is used and yields simple matrix products for the solution of successive 2D uncoupled Helmholtz and Poisson equations at each time step.

The Spectral Vanishing Viscosity (SVV), first introduced by Tadmor (1989) for stabilizing the solution of the inviscid Bürgers equation, is incorporated into the cylindrical Navier-Stokes equations. A viscosity kernel operator, only active for high wave numbers of the numerical approximation, is incorporated in the Helmholtz equations of velocity prediction. Then, the diffusion and SVV terms are combined in order to obtain a new diffusion operator that can be easily written in 1D:

$$\nu \Delta_{SVV} V_N = \nu \Delta V_N + \varepsilon_N \partial_x (Q_N \partial_x V_N) \qquad (2)$$

where V_N is the velocity vector approximation and Q_N is the kernel defined in the spectral space as:

$$\hat{Q}_N(\omega_n) = \begin{cases} 0, & 0 \leqslant \omega_n \leqslant \omega_T, \\ \varepsilon_N \exp([(\omega_N - \omega_n)/(\omega_T - \omega_n)]^2), & \omega_T < \omega_n \leqslant \omega_N \end{cases} \qquad (3)$$

where ε_N is the maximum of viscosity, ω_T is the mode after which the spectral viscosity is applied and ω_N the highest mode calculated. Thus, the viscosity kernel is zero on the lower frequencies. There is no direct way to extend the one dimensional definition of the SVV operator to the three-dimensional case. Then, Séverac and Serre (2007) proposed the following definition which has been used here:

$$\nu \Delta_{SVV} V_N = \nu \Delta V_N + \nabla.[\varepsilon_N Q_N (\nabla V_N)] \qquad (4)$$

where ∇V_N is the Jacobian of the vectorial function V_N, and where ε_N and Q_N are the maximum of viscosity and the 1D viscosity operator respectively.

Computational details

The initial condition corresponds to a fluid at rest. No-slip boundary conditions are applied to all walls. There, $V_r=V_z=0$ on all walls, whereas V_θ is fixed at zero on the stator and the shroud and at the local disk velocity Ωr on the rotor and the hub. At the junctions rotor-stator, the tangential velocity component has been regularized by using a boundary function $V_\theta=\exp((1-z)/\mu)$, with $\mu=0.006$ an arbitrary shape parameter independent of the grid size. This function provides a reasonable representation of experimental conditions (Séverac *et al.*, 2007), while retaining spectral accuracy.

As shown previously, the SVV operator is parametrized in each direction by (ω_T, ε_N). According to the theoretical results obtained by Tadmor (1989), good values of such parameters are $\omega_T \approx O(N^{1/2})$ and $\varepsilon_N \approx O(1/N)$, where N is the degree of approximation in each direction. Let's notice that the SVV operator affects at most the two-third of the spectrum on the highest frequencies (ω_T =0) and consequently, DNS results are easily recovered for laminar flows, contrarily to some classical LES techniques as for example with the well-known spectral eddy viscosity model of Kraichnan (1976). The values of ω_T and ε_N used in the present LES are as following: $\omega_T=(2\ N^{1/2}, 5\ N^{1/2}, 4\ N^{1/2})$ in the (r,θ,z) directions respectively and $\varepsilon_N=1/N$ in all directions.

(151×241×81) grid points in the (r,θ,z) directions respectively are sufficient to get grid independent solutions. For the Reynolds number considered here, the calculations have been performed on the half cavity $[0,\pi]$ only. Indeed, due to the required resolution in the tangential direction, comparisons with experimental measurements (Séverac *et al.*, 2007) have shown that this configuration offered the best arrangement between accuracy and confinement regard. The time step is fixed to $\delta t=10^{-5}$. The accuracy in the description of both boundary layers has been checked by calculating the wall normal coordinate, which remains below or around 1 (Séverac *et al.*, 2007). It means that at least, the viscous sublayer is described by five collocation points.

BASE FLOW

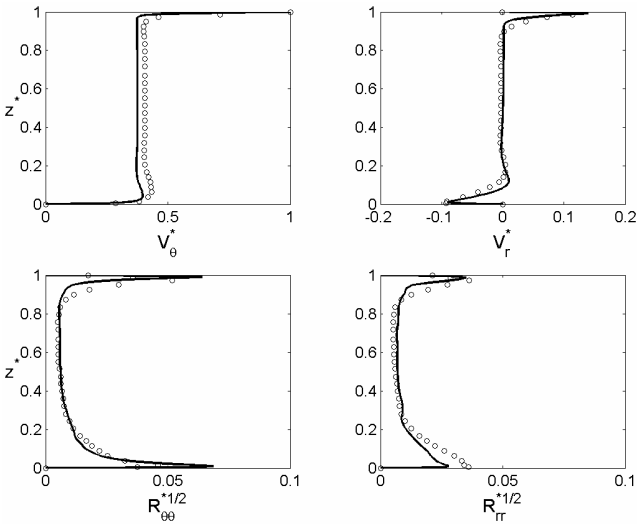

Fig.2: Axial profiles of the mean tangential and radial velocity components and of two normal components of the Reynolds stress tensor for $Re=10^6$ and $r^*=0.7$, in the isothermal case. Comparison between the LES results (lines) and the LDV measurements (circles).

All the quantities have been normalized by the local rotor velocity Ωr. The statistical data have been averaged both in time and in the homogeneous tangential direction. The LES results have been compared to velocity measurements performed at IRPHE using a two-component

laser Doppler velocimeter (LDV) from above the stator (Séverac *et al.*, 2007).

Figure 2 presents the axial profiles of the radial $V_r^* = \overline{V}_r/(\Omega r)$ and tangential $V_\theta^* = \overline{V}_\theta/(\Omega r)$ mean velocity components as well as the associated normal Reynolds stress components $R_{rr}^* = \overline{v'^2_r}/(\Omega r)^2$ and $R_{\theta\theta}^* = \overline{v'^2_\theta}/(\Omega r)^2$ at $r^*=0.7$ in the isothermal case. For this set of parameters, the mean flow corresponds to the regime IV of Daily and Nece (1960): turbulent flows with separated boundary layers. The Ekman layer on the rotor is centrifugal, whereas the Bödewadt layer on the stator is centripetal. They are separated by a central rotating core in solid body rotation. The mean tangential velocity component in the core, known as the entrainment coefficient of the fluid K, is here equal to 0.378. Turbulence is mainly confined in the boundary layers, whereas the core remains almost laminar. The turbulence intensities are rather the same in both boundary layers.

The agreement between the numerical results and the measurements is quite satisfactory for both the mean and turbulent fields. The simulation slightly underestimates the coefficient K with a difference of 6.33% and the peak of R_{rr}^* along the stator. Nevertheless, the LES catches the main features of turbulent rotor-stator flows. The reader is referred to the paper of Séverac *et al.* (2007) for more comparisons and a detailed description of the mean and turbulent fields in the isothermal case.

INFLUENCE OF CENTRIFUGAL BUOYANCY

The influence of the Rayleigh number is here investigated in the case of a highly turbulent flow ($Re=10^6$) of air (Pr=0.7). Instantaneous fields are first presented before quantifying the effect of Ra on the statistical data.

Instantaneous results

The flow is here analysed at $Ra=10^7$. Figure 3 shows iso-values of the instantaneous temperature T and of the instantaneous tangential velocity component V_θ in both boundary layers. Along the cooled rotor (Fig.3a), the structure of the isotherms resembles the one of the iso-values of V_θ (Fig.3b, see also in Séverac *et al.*, 2007). Large positive spiral arms (as they roll up in the sense of rotation of the disk) appear at intermediate radial positions. They are enclosed by two highly turbulent flow regions. The first one is located at the junction between the rotor and the hub. The hot fluid coming from the stator side flows along the hub and impinges the rotor. It is then cooled by this disk. That is the reason why this highly turbulent flow region is characterized by a temperature equal to 0 (in green on Figure 3a). It can be also seen in a (r,z) plane on Figure 4. The second region of high turbulence intensities appears at the periphery of the cavity where the highest values of the local Reynolds number (based on the local radius) prevail. The spiral arms disappeared and more thin structures are created. They are also characterized by a dimensionless temperature close to zero. The cooled fluid coming from the rotor after impingement on the shroud and then on the stator is heated by this lower disk. It creates a crown of fluid with a zero dimensionless temperature at the periphery of the cavity. Afterwards, this fluid flows along the stator from the periphery to the axis of the cavity (as the flow is centripetal in the Bödewadt layer). The fluid is progressively heated until the axis and so higher temperature levels are obtained (Fig.3c,4). The structure of the isotherm maps is more chaotic in this boundary layer. It resembles to the one of the iso-values of V_θ with very thin structures.

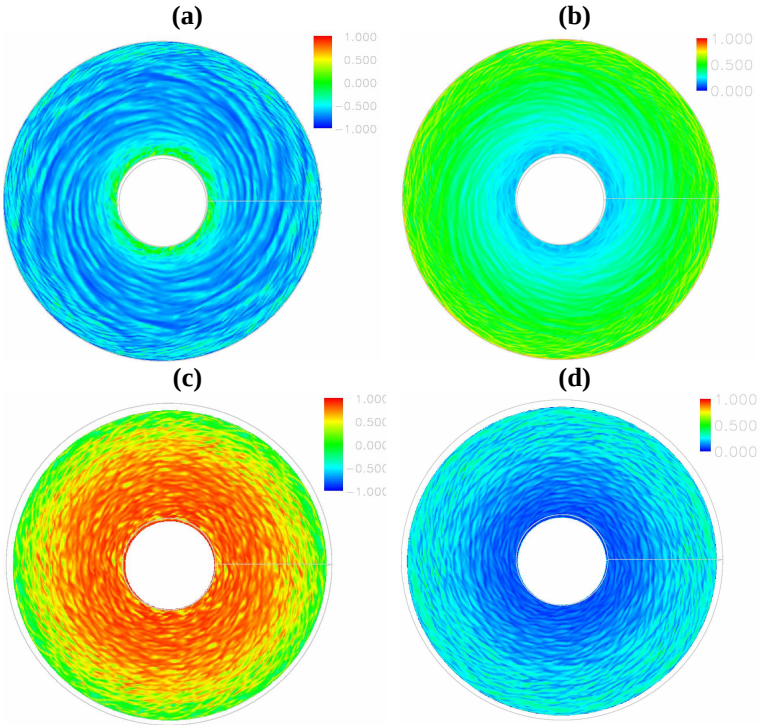

Fig.3: Iso-values at $Ra=10^7$ of the instantaneous temperature T in (a) the Ekman layer (z*=0.99) and (c) the Bödewadt layer (z*=0.01) and of the instantaneous tangential velocity V_θ in (b) the Ekman layer (z*=0.99) and (d) the Bödewadt layer (z*=0.01).

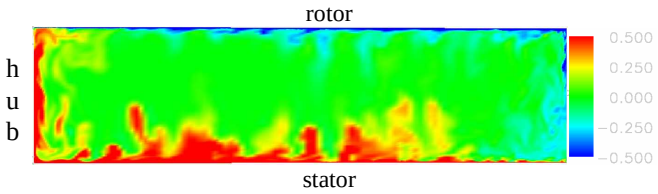

Fig.4: Iso-values of the instantaneous temperature T at $Ra=10^7$ in a (r,z) plane.

Figure 4 confirms that the fluid heated along the stator is carried along the hub and then cooled by the fluid flowing along the rotor. In the same way, the flow cooled by the rotor impinges the shroud and then the stator to be heating. As a consequence, there are two regions along the walls of zero temperature: at the junction between the hub

and the rotor and at the junction between the shroud and the stator. To conclude, the secondary flow in the wall layers is responsible for most of the heat transfers in the cavity. But it can be seen also that thermal convection has also started (Fig.4). Some hot fluid ($T \geq 0.5$) flows indeed from the stator to the rotor with a well defined vertical structure. On the other disk, some cooled fluid ($T \leq -0.5$) is moving down with a small vertical extension. The effect of the heated disk seems to dominate the heat transfers in the cavity.

Statistical data for the flow field

The aim of this section is quantify the effect of the Rayleigh number Ra on the mean and turbulent flow fields for a turbulent air flow (Pr=0.7, $Re=10^6$).

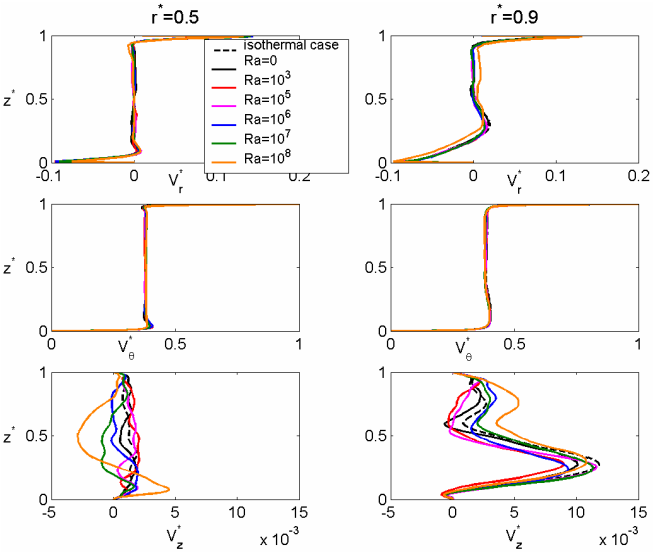

Fig.5: Influence of the Rayleigh number on the mean velocity components at two radial locations r*=0.5 and r*=0.9. Comparisons with the isothermal case.

Figure 5 shows axial profiles of the mean velocity components at two radial locations: $r^*=0.5$ in the similarity area and $r^*=0.9$ close to the shroud where peripheral effects may appear. Six values of the Rayleigh number have been considered and the results are compared to the isothermal case described in Séverac *et al.* (2007). The influence of Ra remains weak as the maximum value of the ratio Ra/Re^2 is equal to 10^{-4}. It confirms the previous results of Serre et *al.* (2004) at lower Reynolds (Re=110000) and Rayleigh ($Ra=2\times10^6$) numbers. The values of the entrainment coefficient (K=0.378 at $r^*=0.5$, K=0.382 at $r^*=0.9$) obtained in the isothermal case remain the same within less than 1.5% at $r^*=0.5$ and within less than 1% at $r^*=0.9$ even for the largest value of Ra. The influence of Ra is more noticeable by looking at the profiles of the mean radial and axial velocity components. Even if there are no significant changes on the maximum of V_r in the Ekman layer, there is a strong modification of the inflow in the Bödewadt layer. At $r^*=0.5$, the minimum of V_r is the same until $Ra=10^6$ and then there is a strong increase of 26.7% for $Ra=10^8$. At $r^*=0.9$, there is a decrease of 14% on the minimum of V_r between $Ra=10^6$ and $Ra=10^8$. For these two radial locations, the axial flow is intensified by an increasing value of Ra even in the core of the flow but note that the values of V_z remain very weak compared to the two other mean velocity components.

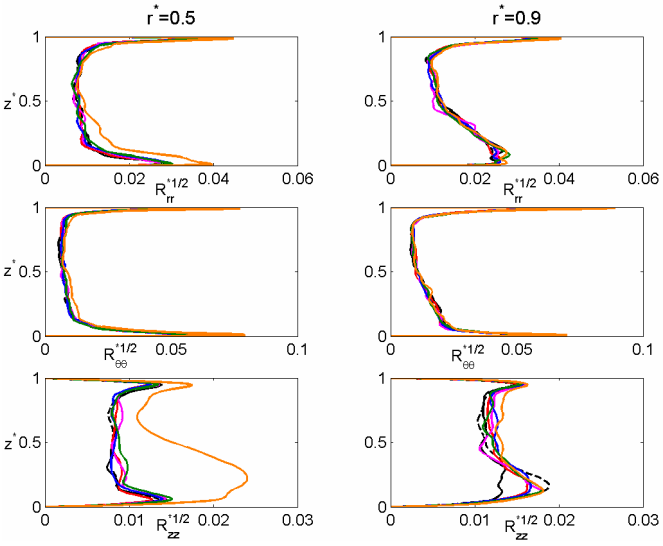

Fig.6: Influence of the Rayleigh number on the normal Reynolds stress tensor components at two radial locations r*=0.5 and r*=0.9. Same legend as Figure 5.

The axial profiles of the three normal components of the Reynolds stress tensor are reported in figure 6 at two radial locations and for six values of the Rayleigh number as in figure 5. The influence of Ra on the turbulent field is more important compared to the one on the mean field. The most noticeable effect is a strong increase by a factor 2 of the axial normal component at $r^*=0.5$ on the stator side. Turbulence intensities increase also with Ra in the boundary layers. The maximum values of the normal stresses increase indeed at least of 7% compared to the isothermal case. There are two exceptions: the maxima of R_{rr} and R_{zz} in the Bödewadt layer at $r^*=0.9$ are almost constant whatever the Rayleigh number. Note that the same behaviors have been observed for $0.3 \leq r^* \leq 0.7$.

Statistical data for the temperature field

Figure 7 exhibits the temperature profiles along the axial direction for six Rayleigh numbers at four radial locations. Whatever the radial location r^*, the temperature is almost constant and equal to zero in the core of the flow. For Ra=0, the thermal boundary layers coincide with the Ekman and Bödewadt layers from the hydrodynamic field. The structure of the thermal field is a Batchelor-like structure. But when Ra is increased, it means when the temperature difference is increased, the axial extension of the core decreases as the thermal boundary layers thicken.

The thickness of the thermal boundary layer on the stator is besides larger than the one on the rotor, which confirms the preponderant influence of the heated disk on the thermal convection in the cavity. In the similarity area $0.3 \le r^* \le 0.7$, the temperature of the fluid at the edge of the stator boundary layer is increased due to the main influence of the heated disk. On the other hand, at $r^*=0.9$ where the cold fluid coming from the shroud (Fig.4) is mixed with the hot fluid flowing along the stator, a small decrease appears in the axial profiles of the temperature.

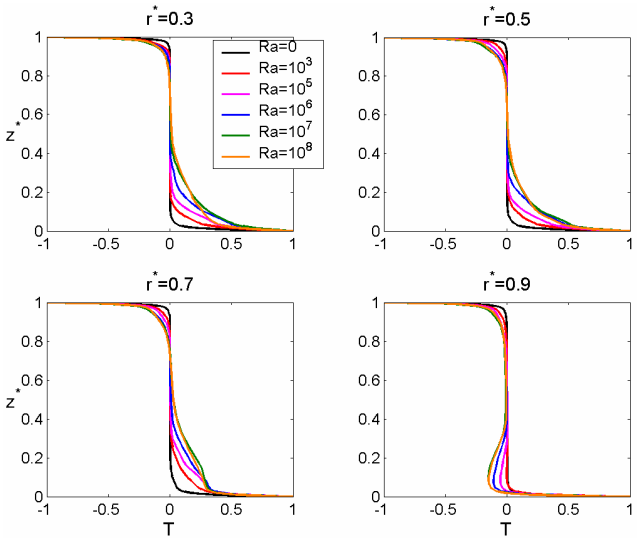

Fig.7: Influence of the Rayleigh number on the mean temperature at four radial locations.

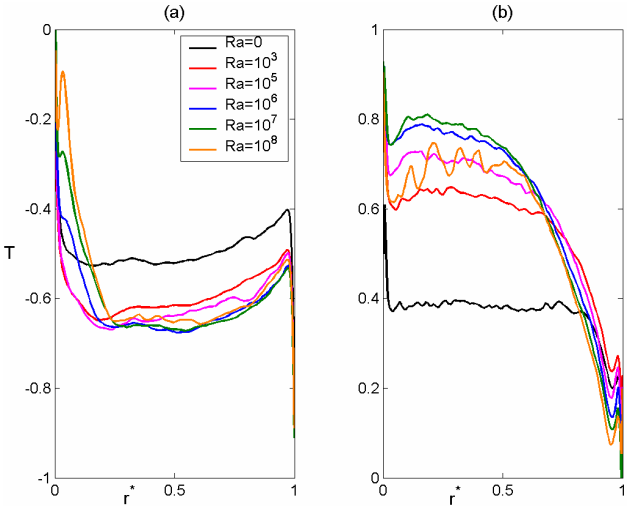

Fig.8: Influence of the Rayleigh number on the radial distribution of the mean temperature T in (a) the Ekman layer (z*=0.99) and in (b) the Bödewadt layer (z*=0.01).

The results of figure 7 are confirmed by the radial distributions of T shown in figure 8 for both boundary layers and the same values of Ra. T slightly increases with the radius along the rotor. On the stator side, T is almost constant close to the axis and strongly decreases towards the periphery. The radial extent of the region of constant temperature decreases rapidly with the Rayleigh number. The magnitude of T is almost constant whatever Ra≠0 and then diminishes for Ra=0. We recall that, in that case, the temperature can be considered as a passive scalar.

Radial distribution of the local Nusselt number Nu

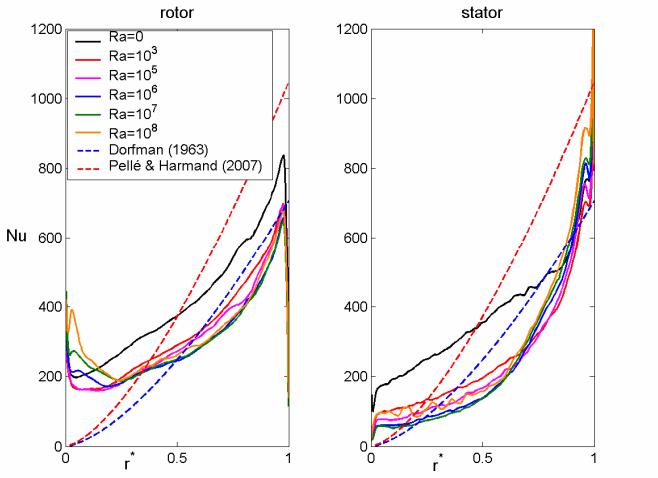

Fig.9: Influence of the Rayleigh number on the local Nusselt number on both disk surfaces.

The effect of the Rayleigh number Ra on the local Nusselt number $Nu=rh_1/\lambda$ (h_1 the convective heat transfer coefficient, λ the fluid conductivity and r the local radius) along the two disks is investigated in figure 9 for given Reynolds $Re=10^6$ and Prandtl Pr=0.7 numbers. Apart from some peripheral effects for r^* very close to 0 and 1, Nu is an increasing function of the radial location. It can be explained for the rotor side by looking at the radial distribution of the relative velocity $V_{rel}^* = \left[(1-V_\theta^*)^2 + V_r^{*2}\right]^{1/2}$ (Fig.10). In the region $0.2 \le r^* \le 0.95$, when moving towards the periphery of the cavity, higher velocities are obtained that enhances the heat transfer coefficient reflected in the Nu values. Moreover the relative velocity is almost constant whatever the Rayleigh number, which may explain the weak influence of Ra on the local Nusselt number. A second explanation has been provided by Dorfman (1963), which showed that the local Nusselt number varies proportionally to the square root of the local Reynolds number $Re_r=\Omega r^2/\nu$ and so varies linearly with the radial location. Along the rotor side, this linear dependence is obtained (see Fig.9) at Ra=0 for $0.145 \le r^* \le 0.68$: $Nu=470\times r^*+160$. The radial extension of this zone decreases when the Rayleigh number increases. On the stator, the linear dependence is obtained at Ra=0 for a much larger radial domain $0.02 \le r^* \le 0.85$: $Nu=440\times r^*+140$. Two cases have to be distinguished: Ra=0 (T is a passive scalar) and Ra≠0. As soon as Ra≠0, there is a strong decrease of Nu in the main part of the cavity. For $10^3 \le Ra \le 10^8$, there is no significant effect of the Rayleigh

number on the radial distribution of Nu apart from at the junction between the rotor and the hub and at the junction between the stator and the shroud where an intense turbulent mixing between cold and hot fluids appears (see also Fig.4). In these zones, Nu increases with the Rayleigh number in agreement with previous results described in Owen and Rogers (1989b).

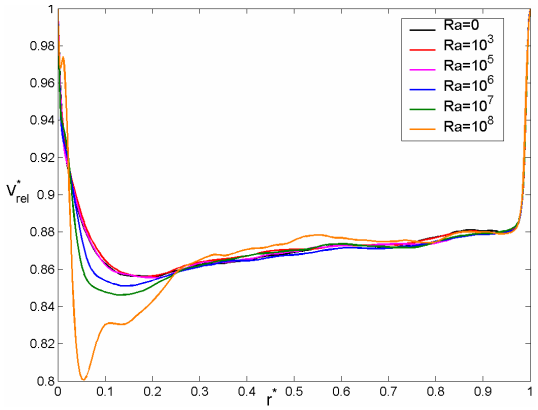

Fig.10: Influence of the Rayleigh number on the radial distribution of the dimensionless relative velocity in the Ekman layer (z*=0.99).

The LES results plotted in figure 9 have been also compared to the empirical correlation laws (5) and (6) given respectively by Dorfman (1963) and Pellé and Harmand (2007):

$$Nu = 0.0197\,(n+2.6)^{0.2}\,Pr^{0.6}\,Re_r^{0.8} \qquad (5)$$

$$Nu = 0.035\,(1-e^{-40H})(1-e^{-4.2\times10^5\,Re})\,Re_r^{0.746} \qquad (6)$$

where H=h/b. For H≥1.05×Re$^{-0.2}$, which is the case here, the local Nusselt number on the rotor is not affected by the presence of a stationary disk (Dorfman, 1963; Owen and Rogers, 1989a). As a consequence, the correlation (5) valid for turbulent flows over a rotating disk can be extended to rotor-stator flows. Harmand *et al.* (1998) provided an estimated value for n=1.04 for turbulent rotor-stator flows. The correlation (5) has been plotted in figure 9 also with n=1.04 but with the local Reynolds number to the power 0.76 instead of the classical value 0.8. With its small modification, the law (5) provides a good estimate for Nu along the stator and also along the rotor at large radial locations. The agreement with the law (6) is not as good as for the correlation (5). The law (6) has been validated for turbulent air flows (Re up to 6.45×10^5) with high interdisk spacing (G≥6.25). For the set of parameters considered here, it gets: $Nu \approx 0.035\,Re_r^{0.746}$, which corresponds to the case of a single rotating disk in still air (Dorfman, 1963). The main discrepancies are attributed to the difference in the temperature distribution law imposed at the disk surfaces. In the experiment of Pellé and Harmand (2007), the rotor is heated and the temperature of the stator is not controlled. Moreover, there are no inner and outer cylinders in their experiment, which explain why the correlation law (6) does not take into account the strong peripheral effects due to confinement.

CONCLUSION

A numerical investigation of turbulent non-isothermal flows within a shrouded rotor-stator cavity has been performed. The highly accurate computation of turbulent rotating flows within finite cavity is of interest for both engineering applications and fundamental research. The results of a Large Eddy Simulation using a 3D spectral code stabilized with a Spectral Vanishing Viscosity model have been firstly favourably compared to velocity measurements for both the mean and turbulent fields in the isothermal case (Séverac *et al.*, 2007).

For Re=10^6 and G=5, the flow is turbulent and exhibits a Batchelor-like structure with two boundary layers separated by an inviscid rotating core, belonging to the regime IV of Daily and Nece (1960). Turbulence is mainly confined in the boundary layers and at the junctions between the rotor and the hub and between the stator and the shroud. Centrifugal buoyancy effects have been then investigated for Rayleigh numbers up to Ra=10^8. Some instantaneous views of the velocity and temperature fields have been provided. It shows that the temperature field is strongly affected by the hydrodynamic structures even at large Ra values. The averaged results show small effects of density variation on the mean and turbulent fields. Some significant effects appear along the stator for Ra=10^8: turbulence intensities are strongly increased in the similarity area. The main features of non-isothermal turbulent rotor-stator flows have been catched by the LES and compared to experimental results (Dorfman, 1963; Harmand *et al.*, 1998, 2000; Pellé and Harmand, 2007). The differences are mostly due, on one hand, to the different temperature distributions imposed at the disk surfaces and to the other hand, to confinement effects, which appear in the present case.

Further computations are still in progress to extend these results for larger values of the Rayleigh number up to 10^{12} but also to investigate the effect of the Prandtl number Pr and provide some empirical correlations for the averaged Nusselt number.

ACKNOWLEDGEMENTS

The authors acknowledge the IDRIS (CNRS) computing centre (program 060242). The authors are very grateful to E. Séverac (MSNM-GP) for fruitful discussions. The work was supported by CNRS in the frame of the DFG-CNRS program “LES of complex flows”.

REFERENCES

K. Abe, T. Kondoh, Y. Nagano, A two-equation heat transfer model reflecting seconf-moment closures for wall and free turbulent flows, *Int. Heat Fluid Flow*, **17**, pp.228-237, 1996.

O. Czarny, H. Iacovides, B.E. Launder, Precessing vortex structures in turbulent flow within rotor-stator disc cavities, *Flow, Turbulence & Combustion*, **69**, 51, 2002.

J.W. Daily, R.E. Nece, Chamber dimension effects on induced flow and frictional resistance of enclosed rotating disks, *ASME J. Basic Eng.*, **82**, pp. 217-232, 1960.

M. Djaoui, R. Debuchy, Heat transfer in a rotor-stator system with a radial inflow, *C.R. Acad. Sci. Paris IIb*, **326**, pp.309-314, 1998.

M. Djaoui, A. Dyment, R. Debuchy, Heat transfer in a rotor-stator system with a radial inflow, *Eur. J. Mech. B/Fluids*, **20**, pp.371-398, 2001.

L.A. Dorfman, *Hydrodynamic Resistance and Heat Loss from Rotating Solids*, Oliver & Boyd, Edinbugh and London, 1963.

S. Harmand, F. Monnoyer, B. Watel, B. Desmet, Local convective heat exchanges from a rotor facing a stator, *Rev. Gén. Therm.*, **37**, pp.885-897, 1998.

S. Harmand, B. Watel, B. Desmet, Local convective heat exchanges from a rotor facing a stator, *Int. J. Therm. Sci.*, **39**, pp.404-413, 2000.

H. Iacovides, J.W. Chew, The computation of convective heat transfer in rotating cavities, *Int. Heat Fluid Flow*, **14 (2)**, pp.146-154, 1992.

R.H. Kraichnan, Eddy viscosity in two and three dimensions, *J. Atmos. Sci.*, **33**, 1521, 1976.

J. M. Owen, R. H. Rogers, *Flow and Heat Transfer in Rotating-Disc Systems – Vol. 1: Rotor-Stator Systems*, Ed. W. D. Morris, John Wiley and Sons Inc., New-York, 1989a.

J. M. Owen, R. H. Rogers, *Flow and Heat Transfer in Rotating-Disc Systems – Vol. 2: Rotating cavities*, Ed. W. D. Morris, John Wiley and Sons Inc., New-York, 1989b.

J. Pellé, S. Harmand, Heat transfer measurements in an open rotor-stator system air-gap, *Exp. Therm. Fluid Sci.*, **31**, pp.165-180, 2007.

S. Poncet, M.P. Chauve, R. Schiestel, Batchelor versus Stewartson flow structures in a rotor-stator cavity with throughflow, *Phys. Fluids*, **17 (7)**, 2005.

S. Poncet, R. Schiestel, Numerical modelling of heat transfer and fluid flow in rotor-stator cavities with throughflow, *Int. J. Heat Mass Transfer*, **50**, pp.1528-1544, 2007.

R. Schiestel, L. Elena, T. Rezoug, Numerical modeling of turbulent flow and heat transfer in rotating cavities, *Numer. Heat Trnasfer A*, **24**, pp.45-65, 1993.

E. Serre, P. Bontoux, B. Launder, Transitional-turbulent flow with heat transfer in a closed rotor-stator cavity, *J. of Turbulence*, **5**, 008, 2004.

E. Séverac, S. Poncet, E. Serre, MP Chauve, Large eddy simulation and measurements of turbulent enclosed rotor-stator flows, *Phys. Fluids*, **19**, 085113, 2007.

E. Séverac, E. Serre, A spectral vanishing viscosity for the LES of turbulent flows within rotating cavities, *J. Comp. Phys*, **226**, pp.1234-1255, 2007.

E. Tadmor, Convergence of spectral methods for nonlinear conservation laws, *SIAM J. Num. Anal.*, **26**, 30, 1989.